

Starbursts and the triggering of the activity in nearby powerful radio galaxies

C. Tadhunter¹, T.G. Robinson¹, R.M. González Delgado², K. Wills¹, R. Morganti³

¹*Department of Physics and Astronomy, University of Sheffield, Sheffield, S3 7RH, UK*

²*Instituto de Astrofísica de Andalucía, Apdo. 3004, 18080 Granada, Spain*

³*ASTRON, PO Box 2, 7990 AA Dwingeloo, The Netherlands*

ABSTRACT

We present high quality long-slit spectra for three nearby powerful radio galaxies – 3C293, 3C305, PKS1345+12. These were taken with the aim of characterising the young stellar populations (YSP), and thereby investigating the evolution of the host galaxies, as well as the events that triggered the activity. Isochrone spectral synthesis modelling of the wide wavelength coverage spectra of nuclear and off-nuclear continuum-emitting regions have been used to estimate the ages, masses and luminosities of the YSP component, taking full account of reddening effects and potential contamination by activity-related components. We find that the YSP make a substantial contribution to the continuum flux in the off-nuclear regions on a radial scale of 1 – 20 kpc in all three objects. Moreover, in two objects we find evidence for reddened post-starburst stellar populations in the near-nuclear regions of the host galaxies. The YSP are relatively old (0.1 – 2 Gyr), massive ($10^9 < M_{YSP} < 2 \times 10^{10} M_{\odot}$) and make up a large proportion ($\sim 1 - 50\%$) of the total stellar mass in the regions of galaxies sampled by the observations. Overall, these results are consistent with the idea that AGN activity in some radio galaxies is triggered by major gas-rich mergers. Therefore, these radio galaxies form part of the subset of early-type galaxies that is evolving most rapidly in the local universe. Intriguingly, the results also suggest that the radio jets are triggered relatively late in the merger sequence, and that there is an evolutionary link between radio galaxies and luminous/ultra-luminous infrared galaxies.

Key words: galaxies:active – galaxies:individual

1 INTRODUCTION

Powerful radio sources are invariably associated with early-type host galaxies and their luminous emission lines and powerful radio emission make them stand out at high redshifts. Therefore, they are potentially unique probes of the evolution of massive early-type galaxies in the early universe. However, if we are to use them in this way, it is crucial to understand the link between the quasar/jet activity and evolutionary processes in the host galaxies. In this context it is notable that the evolution of the co-moving number density of powerful radio sources (Dunlop & Peacock 1990), shows a marked similarity to that of the evolution of the global star formation rate in the universe (Madau et al. 1996). This suggests that the triggering of the quasar/jet activity is intimately linked to the evolution of the general galaxy population.

Observations of powerful radio galaxies in the local universe provide important clues to the triggering mechanism for the jet and quasar activity. In particular, the imaging

studies of Heckman et al. (1986) and Smith, Heckman & Illingworth (1989) provide evidence for morphological features such as double nuclei, arcs, tails and bridges which suggest that, in a substantial subset of radio galaxies, the AGN activity is triggered by the accretion of gas during galaxy mergers and interactions. This is backed up by spectroscopic studies (Tadhunter et al. 1989, Baum et al. 1990) which show emission line kinematics consistent with an accretion origin for the warm gas in many radio galaxies, although a cooling flow origin is a viable alternative to mergers for some objects at the centres of galaxy clusters.

An attraction of the merger hypothesis for the triggering of the activity is that, potentially, it can help to explain the redshift evolution of the radio source population and its similarity to that of the star formation history of the universe. This is because, in a hierarchical galaxy evolution scenario, galaxy mergers and interaction are not only a major driver for star formation, but they can also provide the fuel for AGN and jet activity (e.g. Kauffmann & Haehnelt

2000). Thus, radio galaxies may represent a particular, post-merger phase, in the evolution of giant elliptical galaxies.

Despite the promise of the merger hypothesis for the triggering of the activity, the following uncertainties remain:

- What types of mergers or galaxy interactions trigger radio jet activity?
- At what stage during the merger are the jets triggered?
- Do all massive early-type galaxies go through one or more radio galaxy phase(s) as they build up via galaxy mergers?
- What is the relationship between powerful radio galaxies and other types of merging systems in which a massive early-type galaxy is the end point, for example, the ultraluminous infrared galaxies (ULIGS)?

Unfortunately the quantitative information that can be extracted from the existing morphological and kinematical data is limited. Therefore it is important to develop alternative techniques for investigating the triggering events. One promising alternative is to use the properties of the starbursts that are expected to be triggered as part of the merger process.

Although a substantial proportion of radio galaxies show blue or UV excesses compared with normal early-type galaxies (Lilly & Longair 1984, Smith & Heckman 1989), various activity-related components can contribute to the optical/UV continuum and thereby complicate the interpretation of the continuum spectral energy distributions (SEDs) in terms of the underlying stellar populations. Activity-related continuum components include: scattered AGN light (e.g. Tadhunter et al. 1992, Cimatti et al. 1993, Cohen et al. 1999), nebular continuum from the emission line nebulae (Dickson et al. 1995) and direct light from moderately extinguished quasar nuclei (Shaw et al. 1995). However, with careful modelling of spectroscopic and polarimetric data it is possible to accurately quantify the contributions of these components to the optical/UV continua and thereby study the underlying stellar populations of the host galaxies. In this way it has been possible to show that young stellar populations (YSP) make a significant contribution to the optical/UV continua in 25 – 40% of powerful radio galaxies at low and intermediate redshifts ($z < 0.7$: Aretxaga et al. 2002, Tadhunter et al. 2002, Wills et al. 2002, 2004).

A further complicating factor is that, even if young stellar populations can be identified, they are not necessarily related to the normal evolution of the host galaxies. It has been proposed that the shocks induced by the radio jets as they sweep through the ISM of the host galaxies may trigger star formation, and be a major cause of the alignment effect in high redshift radio galaxies (e.g. Rees 1989). However, apart from a few well-publicised examples in which there is good evidence that the excess UV emission along the radio axis is due YSP rather than scattered light or nebular continuum (e.g. Minkowski's object: van Breugel et al. 1985), direct observational evidence for jet-induced star formation is lacking in the overwhelming majority of radio galaxies.

In order to realise the full potential of radio galaxies as evolutionary probes, it is now important to establish the detailed properties of their YSP. In this, the first in a series of papers in which we will investigate the nature of the YSP in radio galaxies, we present the results of the detailed

Object	z	Galactic $E(B - V)$	Radio axis PA	Slit PA	Exposure time(s)
3C293	0.045	0.017	90	60	2400
3C305	0.041	0.026	44	240	3600
PKS1345+12	0.122	0.034	160	160	2400

Table 1. Basic data and observational details for the objects in the sample. Radio axes in the case of 3C293 & 3C305 are determined from the large-scale radio jets, the Galactic reddening estimates are taken from Schlegel et al. (1998), and the exposure times refer to both red and blue arms of ISIS.

analysis of the continuum spectra of three nearby powerful radio galaxies — 3C293, 3C305, PKS1345+12.

We assume the cosmological parameters $H_0 = 75 \text{ km s}^{-1} \text{ Mpc}^{-1}$ and $q_0 = 0.0$ throughout this paper. For these parameters 1.00 arcsecond corresponds to 0.82, 0.75 and 1.98 kpc at the redshifts of 3C293, 3C305 and PKS1345+12 respectively.

2 THE SAMPLE

The three galaxies chosen for this study have the following features in common: they all show previous spectroscopic, photometric and/or far-IR evidence for recent star formation activity; they all show clear morphological evidence for galaxy mergers/interactions; and they all have compact steep spectrum radio cores, with evidence for strong HI absorption. We further note that all three objects are in relatively low density galaxy environments: isolated or groups rather than clusters. Although they do not represent an unbiased sub-set of the general population of powerful radio galaxies in the local universe, they comprise a useful sample for investigating the links between star formation and the triggering of the radio activity in galaxy mergers. Some basic information about the sample objects is given in Table 1, while a more detailed description of each object is given below.

A further advantage of the objects in our sample is that the AGN contribution to the optical/UV continuum is small in most apertures for most objects. The emission line equivalent widths provide an indication of the contribution of both the nebular continuum (Dickson et al. 1995) and scattered AGN components (see Tadhunter et al. 2002) to the optical/UV continuum. On the basis of small emission line equivalent widths we expect the contribution of AGN-related continuum components to be minor in all spatial regions for 3C293, in the extended apertures for 3C305, and the in extended aperture for PKS1345+12. In the case of the nuclear region of 3C305, the low polarization detected in the imaging polarimetry observations of Draper et al. (1993) provides evidence that the contribution of scattered light is relatively small.

2.1 3C293

Although 3C293 ($z = 0.045$) is an FR II radio source with a total extent of more than 160 kpc, it also shows a compact steep spectrum core, with a complex structure and strong HI 21cm absorption (Baan & Haschik 1981; van Breugel et al. 1984). The impact of the activity on the ISM of the

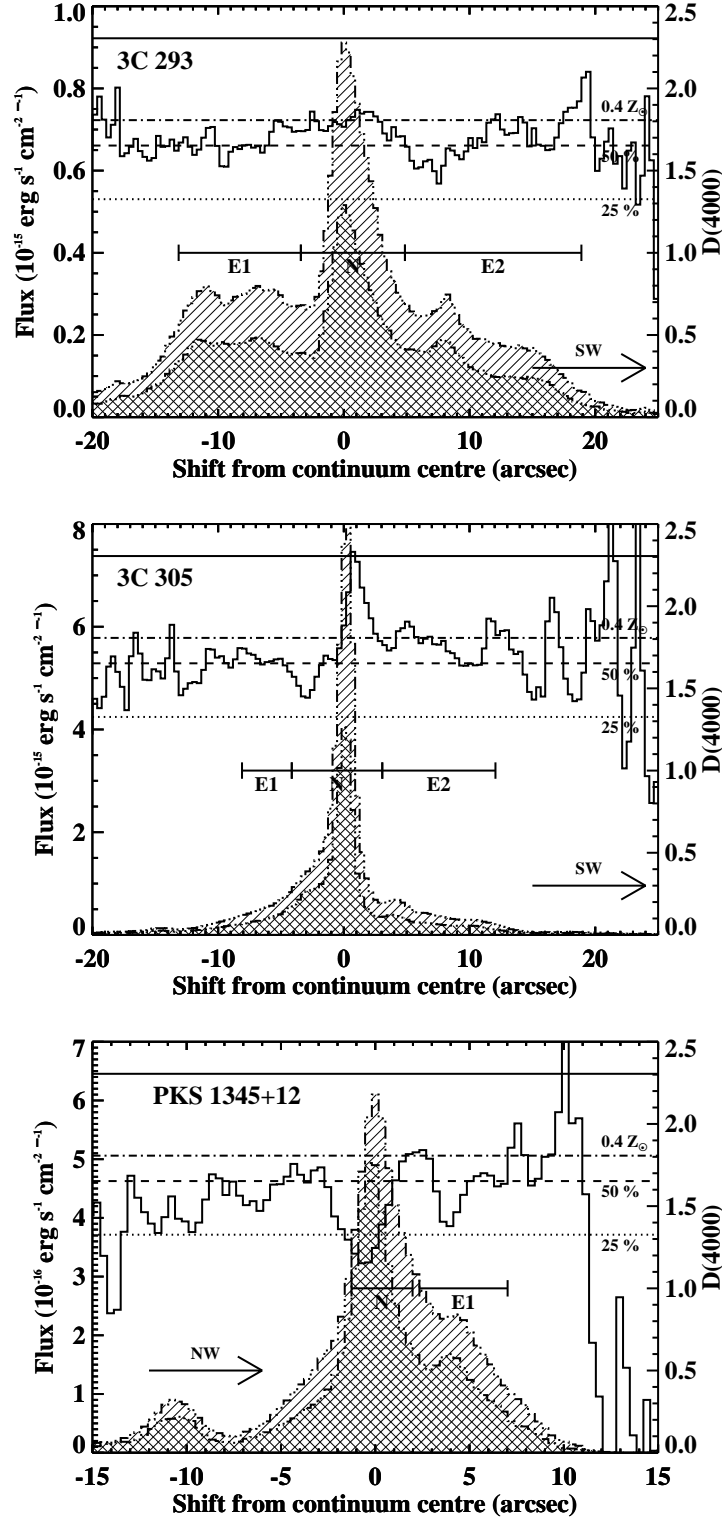


Figure 1. Spatial profiles of the continuum flux integrated in the wavelength ranges 3750 – 3850 Å (cross hatching) and 4150 – 4250 Å (hatching) for 3C 293, 3C 305 & PKS 1345+12. Also shown is the ratio of the two ($D(4000)$, solid line), and the values of this ratio expected for a 12.5 Gyr elliptical with 100% featureless continuum in the 3800 Å bin (dashed line) and with 75 % featureless continuum (dotted line). The value expected for a sub-solar metallicity ($Z = 0.4Z_{\odot}$) elliptical is shown as a dot-dash line.

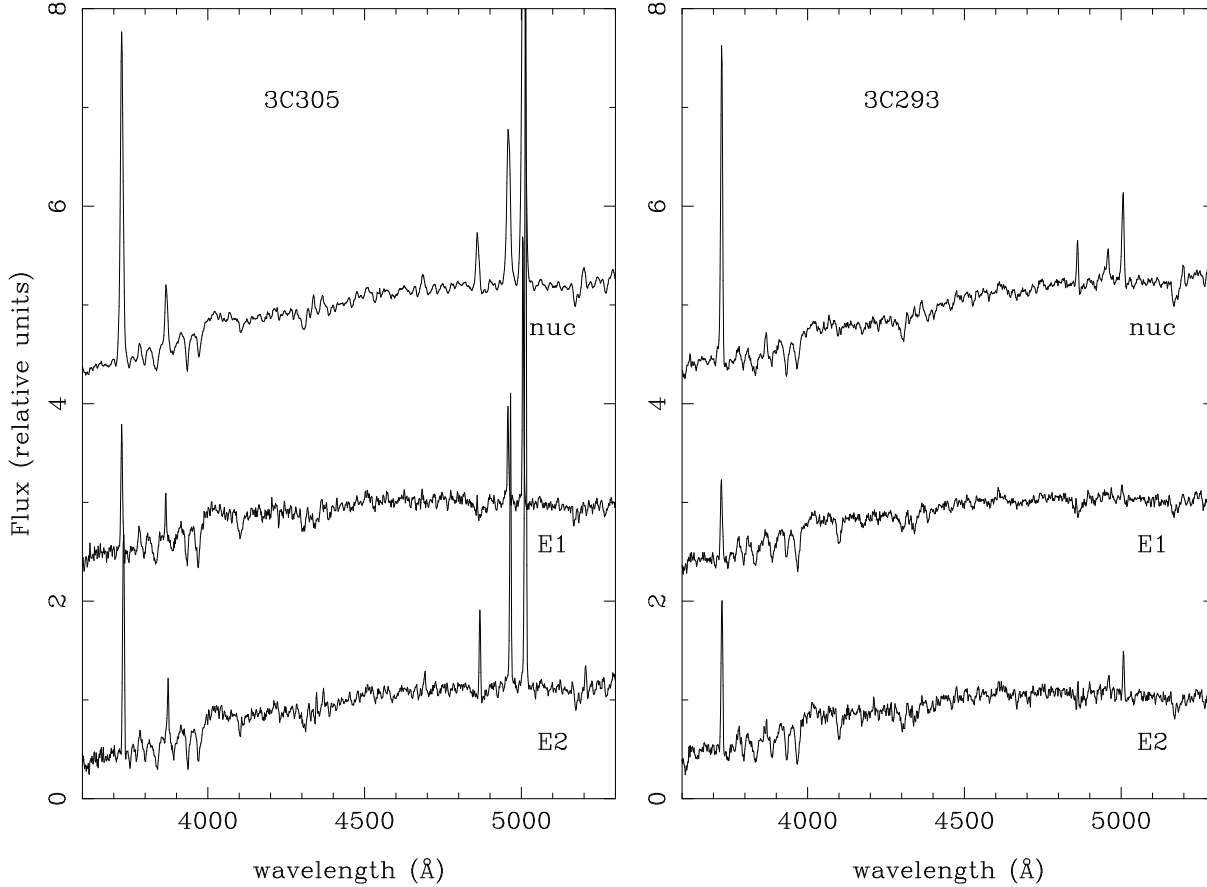


Figure 2. Extracted spectra for the extended and nuclear regions in 3C305 and 3C293. See Figure 1 for a definition of the apertures used to extract the spectra. Only the rest-frame blue/green part of the spectrum is shown in each case. Note that the age sensitive H δ line at 4100 Å, is clearly detected in several of the apertures.

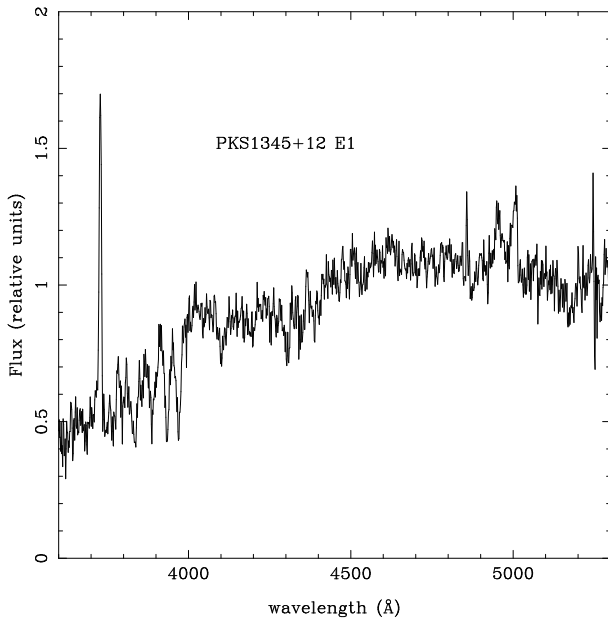


Figure 3. Extracted spectrum for the extended region in PKS1345+12. See Figure 1 for a definition of the aperture used to extract the spectrum. Only the rest-frame blue/green part of the spectrum is shown.

host galaxy is manifest in the broad, blueshifted features detected in both low ionization optical emission lines and HI 21cm absorption. These latter features provide evidence of AGN-induced outflows (Morganti et al. 2003).

As a powerful FRII radio galaxy 3C293 is unusual in the sense that it shows a disk-like morphology in optical images (van Breugel et al. 1984). This, along with the fact that its nuclear regions are crossed by a complex system of dust lanes, suggests an S0 morphological classification. However, on a larger scale the host galaxy shows a jet-like feature linking it to a nearby companion galaxy 28 kpc to the SW, as well as a fan or tidal tail feature extending 50-60 kpc to the west beyond the companion (Heckman et al. 1986). Optical images also show that this object is in an isolated galaxy environment; there are no galaxies brighter than $M_v = -19.4$ within 130 kpc. (Smith & Heckman 1990).

Before the current study, the evidence for recent star formation in this object was indirect, comprising: a modest far-IR continuum excess ($L_{\text{ir}} \sim 2.3 \times 10^{10} L_{\odot}$), bluer (B-V) colours than expected for an elliptical galaxy at this redshift (Smith & Heckman 1989), and ultraviolet imaging observations with the HST that show clumpy structures characteristic of young star clusters (Allen et al. 2002). Perhaps linked to the recent star formation in this source is the detection of strong, extended CO emission and absorption close to the core. Making standard assumptions, the total implied mass

of molecular gas is $\sim 1.5 \times 10^{10} M_{\odot}$ within a radius of 1.5 kpc of the nucleus of the galaxy (Evans et al. 1999a).

2.2 3C305

Unlike 3C293, the radio emission of 3C305 ($z = 0.041$) is relatively compact and shows a distorted “H” morphology. This, and the disturbed kinematics of the optical emission lines, provide evidence that the radio jets are interacting strongly with the ISM in the host galaxy (Heckman et al. 1982).

In most other respects 3C305 is similar to 3C293, with a disk-like optical morphology, complex dust lanes, evidence for tidal tails (Heckman et al. 1986), blue optical colours (Smith & Heckman 1989), a modest far-IR excess ($L_{\text{ir}} \sim 2.0 \times 10^{10} L_{\odot}$), an isolated galaxy environment (Smith & Heckman 1990), and evidence for a rich gaseous environment provided by strong HI 21cm absorption (Jackson et al. 2003). This object had the best prior evidence for recent star formation in the sense that Heckman et al. (1982) reported the presence of Balmer absorption lines characteristic of young stellar populations.

2.3 PKS1345+12

The dominant radio emission of PKS1345+12 ($z = 0.122$) is more compact than that in the other two sources, with total diameter of only 0.15 arcseconds (Stanghellini et al. 2001). Strong HI 21cm absorption is detected against this compact radio structure, which has a distorted jet-lobe morphology (Mirabel 1989, Morganti et al. 2004). Recent optical spectroscopy provides clear evidence for a powerful outflow in the reddened, near-nuclear emission line regions of the western nucleus, perhaps indicating that a strong jet-cloud interaction is taking place (Holt et al. 2003).

The optical morphology of PKS1345+12 differs from that of the other two objects in the sense that it shows a double nucleus (separation ~ 3.6 kpc) surrounded by an elliptical-like envelope (Axon et al. 2000). As well as the double nucleus, the presence of spectacular tidal tails extending out to a radius of ~ 50 kpc provides further evidence that this source has been involved in a major galaxy interaction or merger in the recent past (Heckman et al. 1986). Also based on optical imaging studies, the work of Zirbel (1997) demonstrates that galaxy environment of this source is isolated – at the lower end of the distribution of the $N_{0.5}^{-19}$ environmental richness parameter (see Allington-Smith et al. 1993 for a definition).

Prior to this study, the main evidence for recent star formation in this source comprised the imaging study of Surace et al. (1998) which showed evidence for young star clusters in the extended halo of the system. In addition, measurements by the IRAS satellite reveal the presence of large far-IR continuum excess ($L_{\text{ir}} = 1.1 \times 10^{12} L_{\odot}$). Indeed, PKS1345+12 is one of the few radio galaxies in the local universe that qualifies as an ultraluminous infrared galaxy (ULIGs: see Sanders & Mirabel 1996 for definition). In this context it is also notable that CO observations demonstrate the presence of a large reservoir ($\sim 1.6 \times 10^{10} M_{\odot}$) of molecular gas within ~ 2.5 kpc of the primary (western) nucleus (Evans et al. 1999b).

3 OBSERVATIONS AND REDUCTIONS

The three objects were observed in 2001 May using the ISIS dual-beam spectrograph on the William Herschel Telescope on La Palma. By using the R300R grating on the red arm, and the R300B grating on the blue, we were able to cover a large wavelength range at moderate spectral resolution ($\sim 7\text{\AA}$). This large wavelength range provides a “long lever” for the continuum fitting.

The slit was placed along the major axis of optical emission for 3C293 and 3C305, and along the radio axis for PKS1345+12 (see Table 1 for slit PAs). A slit width of 1.3 arcseconds was used throughout. In order to avoid problems with differential atmospheric refraction, the objects were all observed at low airmass and/or with the slit aligned close to parallactic angle. In the case of PKS1345+12 the slit was centred on the more active, western, nucleus.

The data were reduced using IRAF and the Starlink FARGO packages. First bias subtraction was carried out and cosmic rays removed. The spectra were then wavelength-calibrated, corrected for atmospheric extinction and flux calibrated, using the standard stars and arc exposures taken at the same time as the science images. The data were then corrected for both S-distortion and tilt, using stars in the same 2-d frame as the object wherever possible. After correction, the residual offset in the spatial direction between the two ends of the spectra was estimated to be < 0.3 pixels. The blue spectrum was re-sampled to give the same spatial pixel scale as the red, and the red and blue spectra were aligned with each other and shifted back to the rest frame, using the mean redshift measured from the brighter emission lines.

The reduction process resulted in two spectra with useful data in the rest wavelength ranges 3314–6400 and 5891–8200Å. There is excellent agreement between the flux levels of the blue and red spectra in the wavelength region of overlap between the spectra. We estimate a relative flux calibration error of $\sim \pm 5\%$ across the full spectral range of the data, based on several wide-slit observations of flux calibration standard stars taken during the observing run.

4 RESULTS AND ANALYSIS

The analysis of the continuum spectra for the three objects proceeded via three steps: first, using the 4000Å break to assess the degree of UV excess and investigate the spatial distribution of the extended UV emission; second, modelling the shapes of the spectral energy distributions using a combination of stellar and activity-related continuum components; third, making a more detailed comparison between the data and the models using the CaIIK and Balmer absorptions lines. Because they were carried out independently, each of these three steps will now be described in turn.

4.1 The 4000Å break

To gain an impression of the magnitude of the UV excess in the sample objects, spatial slices of the continuum on each side of the 4000 Å break in each source were extracted. These are shown in Figure 1, along with their ratio, $D(4000)$ — a measure of the 4000Å break amplitude. We use the definition of $D(4000)$ given in Tadhunter et al. (2002):

$$D(4000) = \frac{\int_{4150}^{4250} F_{\lambda} d\lambda}{\int_{3750}^{3850} F_{\lambda} d\lambda}. \quad (1)$$

This form is better suited to active galaxies than the original form of Bruzual(1983), since it is not subject to contamination by bright emission lines such as [NeIII] λ 3869. Moreover, $D(4000)$ is relatively insensitive to the effects of reddening, unlike broad-band colours (e.g. Smith & Heckman 1989), and is not sensitive to redshift (K-correction) effects.

For comparison, Figure 1 also shows the value of $D(4000)$ expected for a solar-metallicity 12.5 Gyr elliptical template spectrum taken from the 1996 version of the Bruzual & Charlot (1993) spectra synthesis models (hereafter BC96: see Charlot et al. 1996 for a discussion). As with the template ellipticals used in the continuum modelling (see below), this template assumes a Salpeter (1955) initial mass function (IMF) formed in an instantaneous burst, with solar metallicity stars in the mass range $0.1M_{\odot} \leq M \leq 125M_{\odot}$. Also shown are values calculated by diluting this old elliptical continuum with a flat spectrum, such that the old elliptical flux comprises 50% and 25% of the flux in the wavelength bin centred at 3800 Å, and the value obtained for a sub-solar metallicity ($Z = 0.4Z_{\odot}$) 12.5 Gyr elliptical. This latter clearly demonstrates that low metallicities are required to produce the same effect as dilution by a flat spectrum. In fact, studies of normal ellipticals, using absorption-line indices, show that their metallicities are generally solar or super-solar (e.g. Kuntschner & Davies 1998), and it is therefore difficult to explain the UV excess in terms of sub-solar abundances.

All three objects in the sample show a significant excess of UV flux, when compared with a passively evolving old elliptical; values of $D(4000)$ suggest that only 25–50 % of the flux in the UV is due to the 12.5 Gyr stellar population. In all cases, the excess is spatially extended, and only the nucleus of 3C 305 shows a value of $D(4000)$ consistent with an old stellar population. Tadhunter et al. (2002) found $D(4000)$ in the range $\sim 1.2 - 2.6$ for a large sample of 2Jy radio galaxies in the redshift range ($0.02 < z < 0.7$). Our measured values of $D(4000)$ are somewhat to the lower end of this range, suggesting a large contribution from YSP or activity-related continuum on radial scales of 1 – 20 kpc.

Various spatial regions of interest were identified in each object using the continuum spatial profiles. These are marked in Figure 1. The spectra of these spatial regions were then extracted from the 2-d frames and used in the continuum modelling process detailed below. The extracted spectra for the blue/green spectral range are shown in Figures 2 & 3.

4.2 Continuum modelling

Following the clear detection of UV excesses in all the sample objects, the nature of the optical/UV continua were investigated by modelling the detailed shapes of the continuum spectral energy distributions (SEDs: see Tadhunter et al. 1996, Robinson et al. 2000). Note that we use SED modelling rather than absorption line indices for this work, because most of the age-sensitive diagnostic absorption lines are strongly affected by emission line infilling (CaII K is an exception — see section 4.3 below). Initially, a nebular continuum was generated for each of the spatial re-

gions, comprising the blended higher ($>H8$) Balmer series, together with a theoretical nebular continuum (a combination of free-free emission, free-bound recombination and two-photon continua) generated using the Starlink software DIPSO. This was then subtracted from the data prior to the modelling (see Dickson et al 1995). For some of the data (notably the nucleus of PKS 1345+12), $H\beta$ has a multiple-Gaussian line profile; in this case separate nebular continua were generated with the same redshift and line width as each emission component. For all but the nuclear region in PKS1345+12 the contribution of nebular continuum to the UV continuum was found to be relatively small ($<10\%$).

After subtraction of the nebular continuum, four sets of models of increasing complexity were fitted to the data. As before, all the stellar population models used in the fitting assume a Salpeter IMF, solar-metallicity instantaneous starburst. First, a model comprising a 12.5 Gyr elliptical template taken from BC96 (see section 4.1) was fitted to the data. Second, models were constructed from two components: a power-law of the form $F_{\lambda} \propto \lambda^{\alpha}$, taken to represent either direct or scattered AGN light, and a 12.5 Gyr-old elliptical galaxy template. Third, a series of models was constructed that comprise a 12.5 Gyr elliptical and a contribution from a young stellar population (YSP), with the age of the YSP chosen to be in the range 0.01 – 2.5 Gyr. Finally, a set of models that combine an old elliptical, a YSP and a power-law was used.

For the nuclei of 3C 293 & 3C 305, the models with unreddened YSP did not give satisfactory fits to the data (see below). In these cases, a further series of models was generated, comprising an old elliptical (12.5 Gyr) combined with a reddened YSP. In the latter case, YSPs with $0 < E(B - V) < 1.6$ were considered. The Seaton (1979) reddening law was used to redden the YSP spectra.

Continuum bins were selected from a list of possible rest frame bins, chosen to avoid emission lines and atmospheric absorption bands. Typically 40 – 45 bins were selected for each object, with the bins chosen to be as evenly distributed in wavelength as possible, in order to avoid biasing the fits towards a particular wavelength region. A normalising bin, common to all three objects was chosen with the wavelength range 4700 – 4730 Å. The models were then generated by scaling the different components so that the total model flux in the normalising bin was $<125\%$ of the observed flux^{*}. The best-fitting model with each set of components, and for each age of YSP, was determined using a chi-squared minimisation technique over the model and data continuum bins. To ensure reasonable calculation times, the power-law spectral index was limited to the range ($-15 < \alpha < 15$).

For the chi-squared fitting we assumed an error of $\pm 5\%$ in each wavelength bin — consistent with the relative flux calibration error. We find that the flux calibration error dominates over photon counting and sky subtraction errors. Note that, since the flux calibration errors are unlikely to be normally distributed, and are not independent between the data bins, we have not assigned formal confidence intervals on the basis of the reduced chi-squared values for the fits;

* The maximum allowed model flux is greater than 100% of the measured flux to allow for uncertainties in the measured flux and models in the bin.

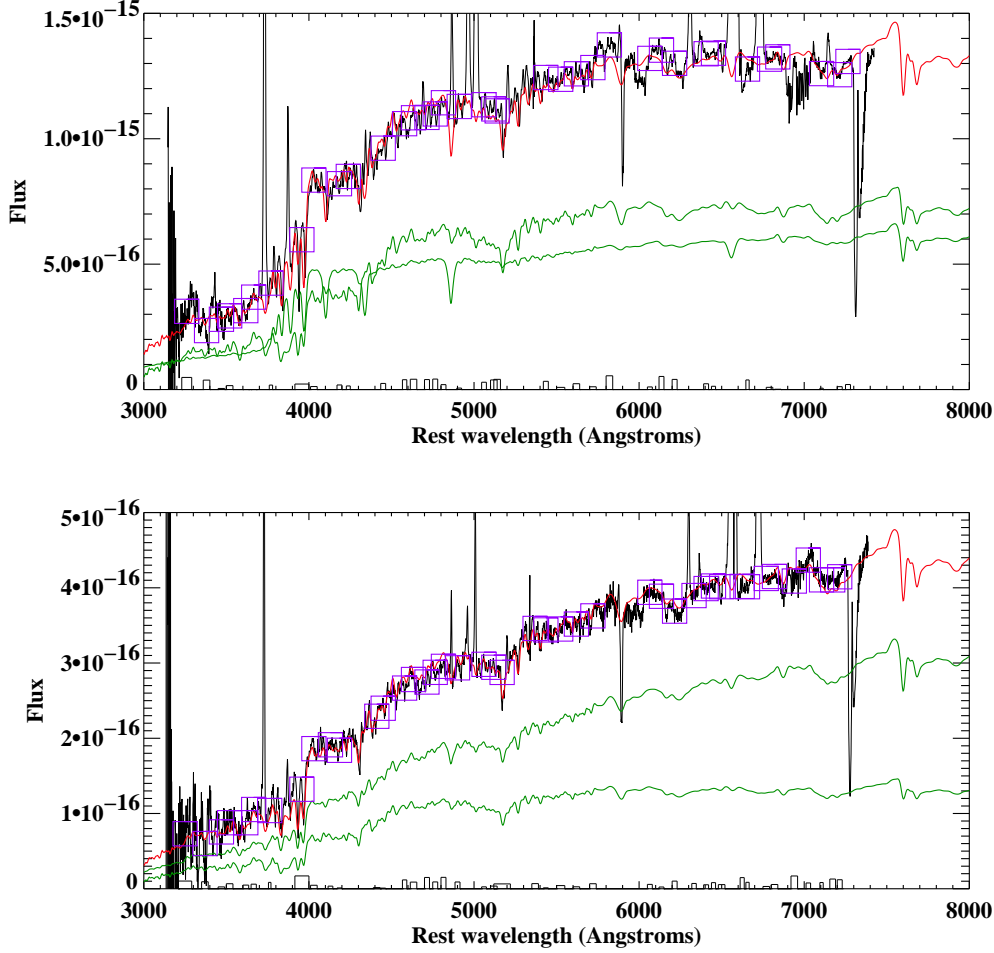


Figure 4. . Examples of model fits to the nuclear spectra of 3C305(top) and 3C293 (bottom), showing the best fitting models superimposed on the data, the data bins, the components to the fits, and the absolute residuals of the data from the models (the latter as rectangular columns at the bottom of the plot). In the case of 3C305 the best fitting model comprises a 12.5Gyr elliptical (54%) plus a 0.4Gyr YSP reddened by $E(B-V)=0.6$ (46%), while in the case of 3C293 the best fitting model comprises a 12.5Gyr elliptical (38%) plus a 2.0Gyr YSP reddened by $E(B-V)=0.4$ (62%), where the percentages refer to the contributions to the total model flux in the normalising bin. Further details of the fitting procedure are given in section 4.2.

the reduced chi-squared values provide an indication of the region of parameter space for the models that provides a good fit to the data, rather than accurate statistical uncertainties. However, it is clear from a visual inspection of the fits that models with $\chi^2_{red} < 1$ give acceptable fits, whereas those with $\chi^2_{red} > 1$ do not provide an adequate description of the spectral shape our high quality data, in the sense that the measured fluxes in several adjacent wavelength bins differ systematically from the model by more than 5% of the total flux. This suggests that the assumed $\pm 5\%$ errors are realistic. On this basis we regard any model with $\chi^2_{red} < 1$ as acceptable.

As examples of our fitting procedure, we show fits to the nuclear spectra of 3C305 and 3C293 in Figure 4, with the continuum bins and residuals from the fits clearly indicated.

We consider the results of the model fits for each object in the following sections.

4.2.1 3C293

Example SED modelling results for 3C293 are presented in Figures 4, 5 & 6 and Table 2.

For the two extended apertures in 3C293 (E1 and E2) we find that the optical SEDs can only be fitted adequately if we include a YSP component that contributes between 20 and 100% of the light in the normalising aperture (depending on the age of the YSP). Inclusion of a power-law component as well as a YSP improves the fits marginally. However, the contribution of the power-law component in the normalising bin is relatively minor, and the power-law slope relatively red, suggesting that the power-law may be compensating for a small amount of reddening and/or inadequacies in the flux calibration.

The ages of the YSP in the extended regions of this object are not well-constrained by the SED modelling alone. We find that, although the SEDs are best fit with YSP ages of ~ 1 Gyr, all YSP ages greater than 0.075 Gyr produce an

	OE %	YSP %	YSP age (Gyr)	PL %	PL α	χ^2
3C293 E1	54 ± 4	54 ± 5	1	—	—	0.65
	38^{+14}_{-13}	59^{+13}_{-15}	1	8 ± 7	$2.3^{+6.1}_{-1.4}$	0.33
3C293 E2	41 ± 4	64 ± 5	1	—	—	0.50
	33^{+16}_{-14}	64^{+14}_{-15}	1	7 ± 7	$1.5^{+13.4}_{-7.8}$	0.37
3C 293 N	82 ± 10	6^{+7}_{-6}	0.5	17^{+6}_{-7}	$3.0^{+1.1}_{-0.6}$	0.47
3C305 E1	28 ± 4	77 ± 5	1	—	—	0.70
	16^{+17}_{-14}	79^{+15}_{-18}	1	8 ± 8	$1.9^{+13.0}_{-2.2}$	0.43
3C305 E2	91 ± 3	17 ± 3	0.5	—	—	1.31
	73 ± 10	25^{+6}_{-7}	0.5	5^{+6}_{-5}	$3.8^{+3.7}_{-1.3}$	0.66
PKS1345+12 E1	21 ± 4	86 ± 5	1	—	—	0.54
	21^{+5}_{-14}	74^{+13}_{-12}	1	4^{+6}_{-4}	± 15	0.52

Table 2. Best-fitting models to the continuum in selected regions of 3C 293, 3C305 and PKS1345+12 (unreddened YSP only). Percentages are quoted relative to the observed flux in the range 4700 – 4730 Å.

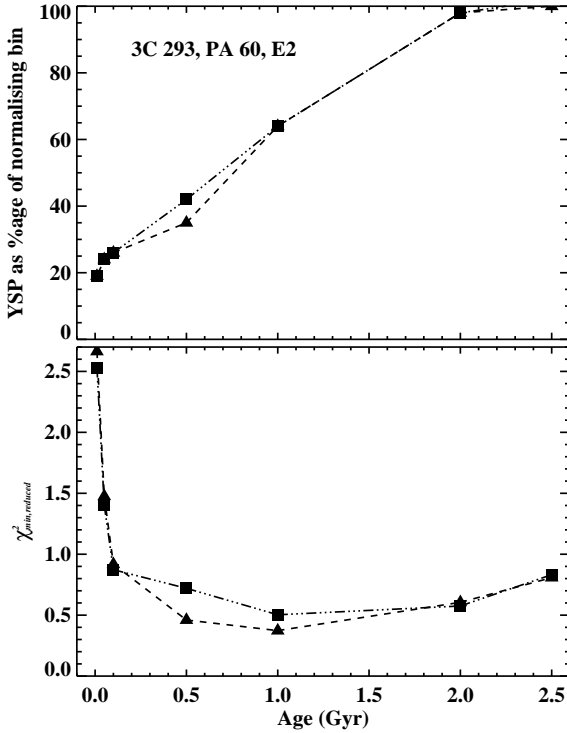


Figure 5. Results of continuum modelling for 3C 293, E2. (Top) Percentage of YSP in best-fitting model at that age vs age of YSP. (Bottom) Value of $\chi^2_{min, reduced}$ vs. age. If $\chi^2 > 1$, fits are not significant. Dot-dash lines denote models without power-law components, dashed lines are models that include a power-law. The points on each line reflect those ages at which models were generated.

acceptable fits to the SEDs (Figure 5). We face the problem that the results are degenerate. For example, the SED modelling does not distinguish between, on the one hand a continuum dominated by an old stellar population plus a moderate contribution from a relatively young YSP (< 0.3 Gyr), and on the other a single intermediate age ($\sim 2.0 - 2.5$ Gyr) stellar population.

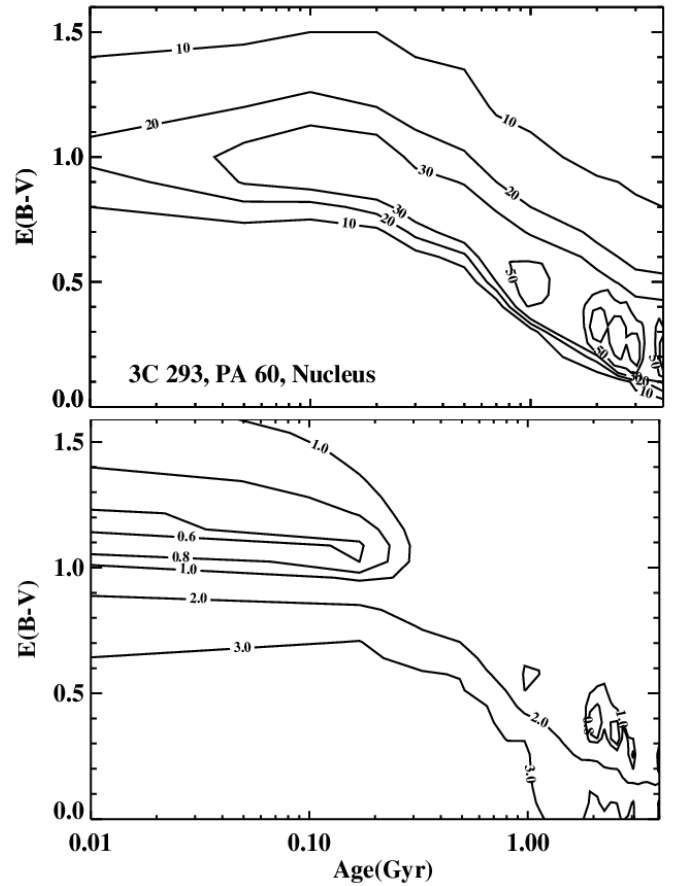


Figure 6. Results of fitting reddened YSPs to 3C 293, nucleus. (Top) Contour plot representing the percentage contribution of the YSP for the best-fitting model at a given age and reddening. (Bottom) Contour plot representing the value of $\chi^2_{min, reduced}$ for the best-fitting model. In both cases, no power-law component is fitted.

In the nuclear regions of 3C293, despite the tentative detection of absorption underlying the Balmer emission lines, a UV excess, and star clusters detected in UV HST images (Allen et al. 2002), the overall continuum SED is relatively red (see Figure 4). Consequently, it is not possible to obtain an acceptable fit to the nuclear SED with models comprising solely an old elliptical plus unreddened YSP; acceptable fits can only be obtained with the inclusion of a significant red ($\alpha \sim 3$) power-law component. However, HST imaging results presented by Chiaberge et al. (1999) show no evidence for a power-law point source component in 3C293, despite the detection of point sources in many of the objects in their sample with fluxes of $\sim 1 \times 10^{-17}$ erg cm $^{-2}$ s $^{-1}$ Å $^{-1}$ at ~ 7000 Å — much smaller than the putative power-law component required by our SED modelling. The redness of the required power-law and the presence of dust lanes in HST images of the nuclear regions suggests an alternative model that comprises a combination of a reddened YSP and an old elliptical galaxy component. The contours of reduced χ^2 shown in Figure 6 allow us to determine which combinations of reddening (parameterised as $E(B-V)$) and YSP age provide an adequate fit to the nuclear continuum. We find that acceptable fits are obtained with an elliptical galaxy component plus either a relatively young YSP (< 0.3 Gyr) with a large reddening ($E(B-V) > 1.0$), or a relatively old YSP (1.0 – 2.5 Gyr) with moderate reddening ($0.3 < E(B-V) < 0.5$).

Therefore, despite the clear presence of YSP in all three apertures modelled for this source, we find that we cannot determine the ages, relative contributions and reddening of the YSP based on the SED modelling alone. In section 4.3 below we discuss a method for breaking this degeneracy, based on the strength of the CaII K absorption line.

4.2.2 3C305

Example SED modelling results for 3C305 are presented in Figures 4, 7 & 8 and Table 2.

Some aspects of the modelling results for 3C305 are similar to those for 3C293. For example, in the extended regions of 3C305 we find that we can obtain a reasonable fit with a model comprising an old elliptical plus a YSP, and can improve the fits with the addition of a red-power law that contributes a relatively small proportion of the flux in the normalising bin. In the extended regions of this object, however, the ages are better constrained than in 3C293, with YSP ages in the range 0.4 – 1.5 Gyr favoured by the models, and YSP ages younger than 0.1 Gyr and older than 2.0 Gyr ruled out (Figure 7).

In the case of the nuclear aperture, we find that no combination of old stellar population, unreddened YSP and power-law, or any of these two components alone can provide an adequate fit to the nuclear spectrum in this source. However, a combination of a reddened YSP plus an old stellar population provides an excellent fit to the nuclear SED for YSP ages in the range $0.2 < t_{YSP} < 1.0$ Gyr and reddening in the range $0.4 < E(B-V) < 0.8$, with a best fit obtained for $t_{YSP} \sim 0.4$ Gyr and $E(B-V) \sim 0.6$ (Figure 8). Note that the age deduced for the YSP in the nuclear regions is consistent with those deduced for the extended regions in this source, and that this object does not suffer from the degeneracy problem noted for 3C293. Nonetheless,

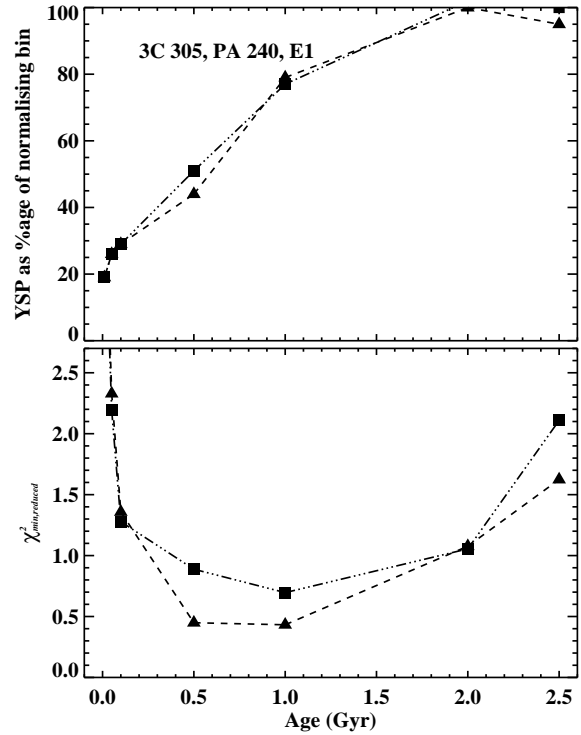


Figure 7. Results of continuum modelling for 3C 305, E1. (Top) Percentage of YSP in best-fitting model at that age vs age of YSP. (Bottom) Value of $\chi^2_{min, reduced}$ vs. age. If $\chi^2 > 1$, fits are not significant. Dot-dash lines denote models without power-law components, dashed lines are models that include a power-law. The points on each line reflect those ages at which models were generated.

in section 4.3 below we will check the results of the SED modelling using CaII K line strength measurements.

4.2.3 PKS1345+12

Example SED modelling results for PKS1345+12 are presented in Figure 9 and Table 2.

The nuclear regions of PKS1345+12 are extremely active, with luminous, highly reddened emission line regions that are undergoing outflow from the nucleus (Holt et al. 2003). Because of the reddening of the emission line regions, it is difficult to subtract the nebular continuum adequately in the nuclear aperture. Moreover, the strength and breadth of the emission lines from the outflowing gas make it difficult to identify sufficient continuum bins for the SED modelling. Overall, the extreme activity precludes accurate stellar population analysis close to the nucleus of this source. Therefore we have concentrated on the extended region centred 5 arcseconds to the north west of the nucleus (E1). In this region we find that we can obtain an accurate fit to the SED with a combination of an old elliptical galaxy plus an unreddened YSP with age in the range $0.5 < t_{YSP} < 1.5$ Gyr (Figure 9). The addition of a power-law component does not significantly improve the fits. Note that this is the first direct spectroscopic detection of a YSP in this source. We check

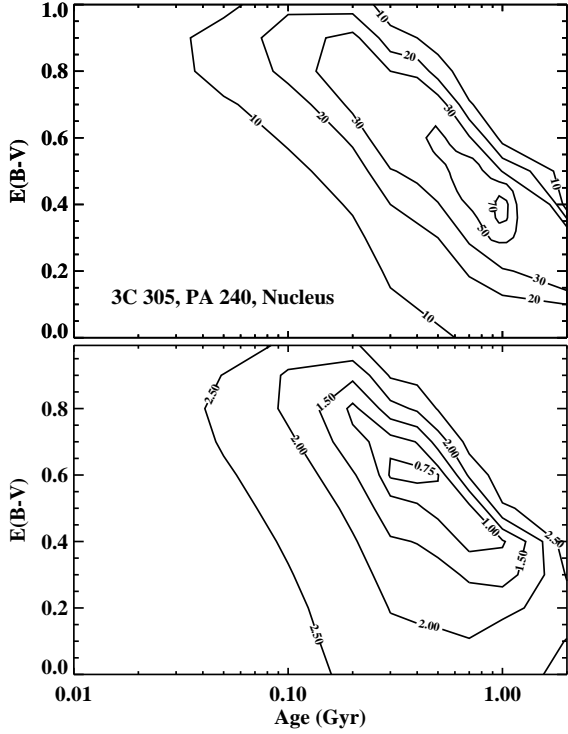


Figure 8. Results of fitting reddened YSPs to 3C 305, nucleus. (Top) Contour plot representing the percentage contribution of the YSP for the best-fitting model at a given age and reddening. (Bottom) Contour plot representing the value of $\chi^2_{min, reduced}$ for the best-fitting model. In both cases, no power-law component is fitted.

the age of the YSP using the CaII K line strength in the next section.

4.3 Line strengths

The SED modelling described above is our primary analysis tool. However, the stellar absorption line features provide useful complementary information which allows us to check the SED modelling results and resolve ambiguities.

First we note that H δ and higher order Balmer lines are detected in absorption in several spatial regions of our objects (see Figure 2), despite the potential for emission line contamination. Since these features are too weak to detect in stellar populations with ages above 5 Gyr, their detection in the radio galaxies provides unambiguous evidence for a significant contribution from young or intermediate age stellar populations (González Delgado, Leitherer & Heckman 1999). This supports one of the major conclusions of our SED modelling.

Useful information on the young stellar populations can also be obtained using the age-sensitive CaII K line, which is not significantly affected by emission line contamination. This line has the potential of allowing us to break the degeneracy between the age and relative contribution/reddening of the YSP in the spectral synthesis results that was noted above.

Since the resolution of the BC96 models is too low for

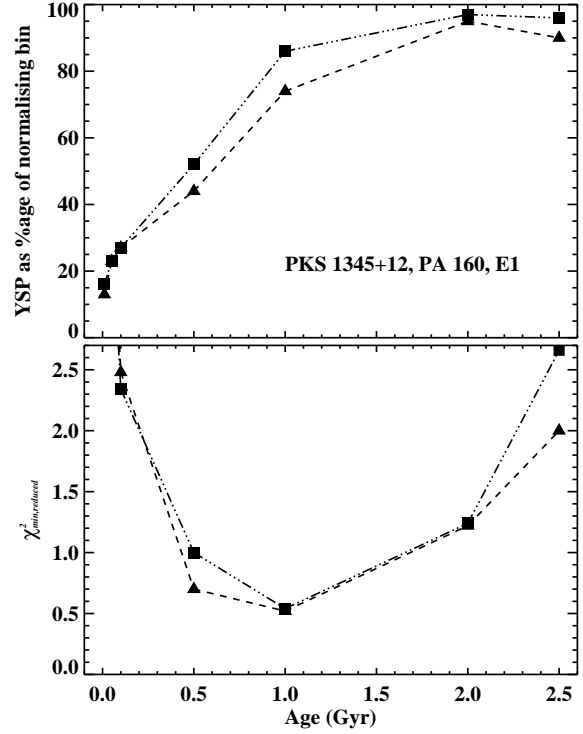


Figure 9. As Figure 5, but for PKS 1345+12, E1.

detailed modelling of absorption features, we have compared our spectra instead with the higher resolution spectral synthesis results of González Delgado et al. (1999, 2001) over a limited spectral range surrounding the Ca II K line. In doing so, we have used the results of the SED modelling from section 4.2 as a guide to the relative age and contribution of the YSP. Because we only consider a narrow spectral range we have not taken into account reddening of the YSP component. The results are shown in Figures 10, 11 & 12.

First we consider 3C293, for which either an elliptical plus a moderate contribution from a relatively young YSP, or an elliptical plus a large contribution from an intermediate age YSP, provide good fits to the SED. In the case of the nuclear aperture of 3C293 we find that the strength of the Ca II K line is underpredicted by the E+young YSP model, however, the E+intermediate age YSP model provides an excellent fit to this line (see Figure 10). Therefore, based on both the SED fitting and the CaII K line strength, we conclude that the age of the YSP required to fit the nuclear spectrum in 3C293 is 1.0 — 2.5 Gyr; in this case we have broken the degeneracy between the age and the reddening/proportional contribution of the YSP. Similar results are obtained for aperture E2, however, in region E1 we find evidence for significantly younger ages, as signalled by the relatively weak CaII K line (see Figure 10, top two plots). In this latter region, the combined SED and CaII K results suggest YSP ages in the range 0.1 — 0.5 Gyr. Note that this model also provides an excellent fit to the H δ line in this region, which is relatively free of emission line contamination.

In the case of 3C305 (see Figure 11), the CaII K results are broadly consistent with the SED modelling, but favour the upper end of the YSP age range derived from the SEDs

(0.6 — 1.0 Gyr in the case of the nuclear aperture); models with YSP ages $t_{YSP} < 0.4$ Gyr underpredict the CaII K line strength.

Finally, in the case of PKS1345+12 E1, we find that the CaII K results are consistent with the YSP ages derived from the SED modelling ($0.5 < t_{YSP} < 1.5$ Gyr), and the model shown in Figure 12, which comprises a 60% contribution from a 0.7Gyr YSP and a 40% contribution from an elliptical, provides an excellent fit to the CaII K line.

4.4 Summary of key results

A summary of the properties of the YSP derived from this study is presented in Table 3. As well as our best estimates of the ages, we provide estimates of the masses of YSP in the regions covered by the slits, and the proportion of the total in-slit stellar mass contributed by the YSP. For the nuclear regions the YSP masses were estimated following correction for reddening. All the estimates of ages and masses are based on the spectral synthesis results of BC96 for an instantaneous starburst, Salpeter IMF with mass range $0.1 - 125 M_{\odot}$ and solar metallicity.

Since we are also interested in the relationship between the YSP and far-IR luminosities in the sample objects, we have estimated the bolometric luminosities for the nuclear YSP, and the amount of far-IR radiation absorbed by the extinguishing dust, for comparison with the measured far-IR luminosities of the targets. The results are shown in Table 4. Using the spectral synthesis models we can also “turn the clock back” and estimate the bolometric luminosities that the nuclear YSP would have had in the past. The results – which are based on the instantaneous burst models of BC96 – are shown in graphical form in Figure 13 for 3C305 and 3C293, where they are compared with the luminosities of luminous- and ultra-luminous infrared galaxies (LIGs and ULIGs: see Sanders & Mirabel 1996 for definition).

The key results from our study are as follows.

- **Ages of the YSP.** The oldest YSP components detected in all three galaxies have post-starburst ages in the range $0.5 < t_{YSP} < 2.5$ Gyr, although there is evidence for a younger YSP in region E1 of 3C293.

- **Reddening.** Unsurprisingly, given the imaging evidence for dust lanes, the YSP detected in the near-nuclear regions of 3C293 and 3C305 are significantly reddened.

- **Masses of the YSP.** The masses of the YSP are substantial, particularly in the nuclear regions of 3C293 and 3C305 where they are comparable to masses of molecular gas estimated on the basis of measurements of CO in the core regions of 3C293 and PKS1345+12 (Evans et al. 1999a,b).

- **YSP contribution to the total stellar mass.** The YSP contribute a substantial proportion of the total in-slit stellar mass in all the regions they are detected, even in the near-nuclear regions where the contribution from the old stellar populations in the galaxy bulges might be expected to be substantial.

- **Current far-IR luminosities.** For 3C305 and 3C293 the YSP luminosities absorbed/scattered by dust are similar to the current far-IR luminosities of the galaxies. This supports the idea that the dust radiating the far-IR light is heated by the post-starburst components detected in our spectra.

- **Past far-IR luminosities** On the basis of the results presented in Figure 13, and assuming complete absorption and reprocessing of the radiant luminosity of the YSP by dust, it is clear that 3C293 and 3C305 would have appeared as ULIGs if observed within 10 Myr of the start of the starbursts. This assumes that the starbursts were instantaneous, however, even for non-instantaneous starbursts, it is clear that these objects would have appeared as LIGs up to 0.1 Gyr after the start of the starbursts, provided that the star formation episode did not last longer than 0.1 Gyr.

4.5 Uncertainties in the derived properties

A major advantage of our SED modelling technique compared with the alternative method of using the absorption line indices is that it allows us to account directly for all the activity-related and stellar components that contribute to the observed spectra. Moreover, because of their wide spectral coverage, our WHT/ISIS data are sensitive to a range of stellar population ages, reddened or unreddened. The complementary information provided by the CaII K line allows us to refine age estimates based on the initial SED modelling. Therefore we are confident about our modelling technique and the suitability of our dataset for studies of this type.

Most probably, the largest sources of uncertainty in the results described above relate to the assumed parameters of the spectral synthesis results used to model the data, most notably, the duration of the starburst, the abundances, and the IMF shape and mass range.

In the above analysis we assumed that the starburst was instantaneous in each region of each galaxy. In reality, the star formation history might have been more complex, with multiple bursts, or continuous star formation. The effect that more complex star formation histories would have on our results can be gauged by considering the extreme case in which, stars have actually formed at a continuous rate, but that we have attempted to model the SED with an instantaneous burst YSP model. A continuous, or quasi continuous, star formation will always produce an SED that is bluer, has a larger UV excess and a smaller Balmer break than an instantaneous burst model of similar age. Therefore, attempting to model such an SED with an instantaneous burst model will always underestimate the time since the start of the star formation episode, and the ages of YSP estimated above will be lower limits on the time since the start of the starbursts. This strengthens the conclusion that the post-starburst YSP in radio galaxies are relatively old.

Considering the issue of the abundances, on the basis of our analysis and the morphological study of Heckman et al. (1986) it is likely that the starbursts have been triggered by the interaction between two or more galaxies, at least one of which is a gas-rich disk galaxy; we can rule out the idea that the activity has been triggered by a minor accretion event such as, for example, the accretion of a dwarf irregular galaxy. Thus we expect that the abundances of the gas out of which the stars form in the starburst are likely to be moderately enriched i.e. close to solar; it is unlikely that our results are affected by abundances that are significantly sub- or super-solar.

Perhaps the most serious uncertainty, however, is the exact shape and mass range of the initial mass function (IMF). An IMF that in reality is steeper than Salpeter, or

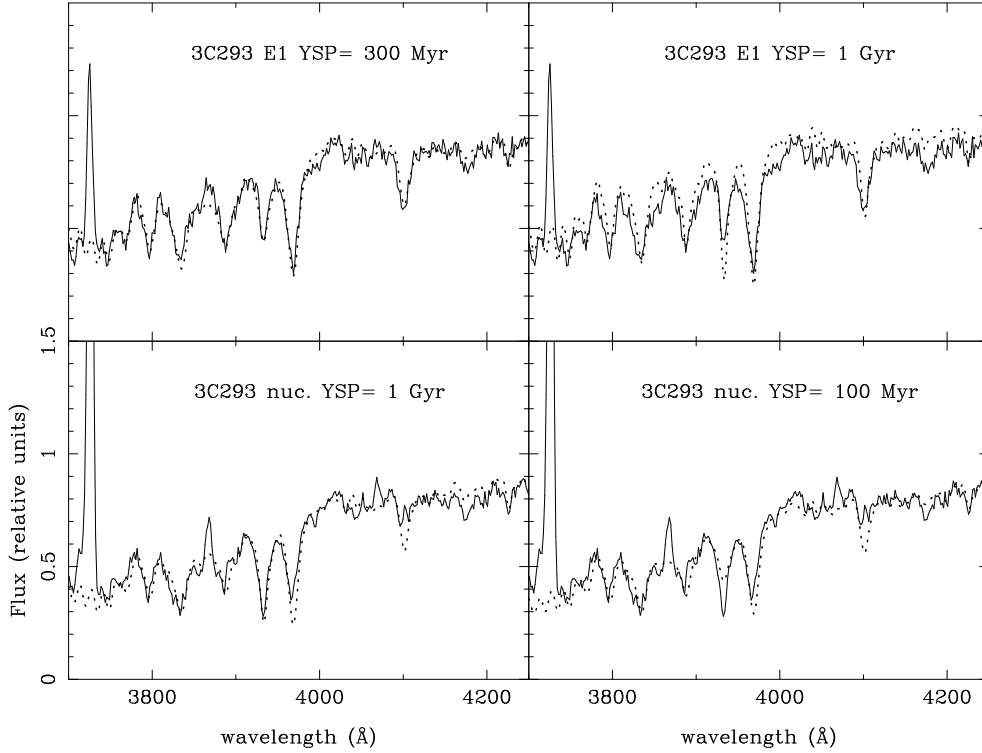


Figure 10. Detailed fits to the nuclear (bottom) and E1 (top) spectra of 3C293 for different YSP contributions and ages. In each case the solid line shows the spectrum of the source, and the dotted line the model fit. The different models are as follows. Lower left: nuclear spectrum with 50% 1 Gyr YSP plus 50% elliptical model. Lower right: nuclear spectrum with 35% 0.1 Gyr YSP plus 65% elliptical model. Upper left: E1 spectrum with 30% 0.3 Gyr YSP plus 70% elliptical model. Upper right: E1 spectrum with 70% 1 Gyr YSP plus 30% elliptical model. The relative proportions of the different components are determined in a normalising bin at 4700Å. The key CaII K feature is at a rest wavelength of 3934Å.

		Age of YSP / Gyr	12.5 Gyr mass / M_{\odot}	YSP mass / M_{\odot}	YSP % of total mass
3C 293	E1	0.1 – 0.5	$(1.0 - 2.6) \times 10^{10}$	$(0.50 - 2.2) \times 10^8$	0.4 – 4.6
	E2	1.0 – 2.5	$(0.0 - 4.9) \times 10^9$	$(0.67 - 3.4) \times 10^9$	12 – 100
	N	1.0 – 2.5	1.0×10^{10}	$(0.80 - 1.1) \times 10^{10}$	44 – 52
3C 305	E1	0.5 – 1.5	$(0.85 - 4.1) \times 10^9$	$(0.88 - 1.9) \times 10^9$	31 – 51
	E2	0.5 – 1.0	$(1.3 - 1.5) \times 10^{10}$	$(1.3 - 4.1) \times 10^8$	0.9 – 3.0
	N	0.4 – 1.0	$(2.6 - 5.6) \times 10^{10}$	$(1.1 - 1.9) \times 10^{10}$	16 – 42
PKS 1345 +12	E1	0.5 – 1.5	$(0.28 - 1.7) \times 10^{10}$	$(0.77 - 3.7) \times 10^9$	4 – 56

Table 3. Ages and masses for the young and old stellar populations for the various spatial regions of the objects. In each case a range of values is given to cover the range of models that give an acceptable fit to the SEDs and CaII K absorption lines. The final column gives the percentage of the total stellar mass contributed by the YSP in the regions covered by the slit.

Object	Bolometric YSP luminosity / L_{\odot}	Absorbed luminosity / L_{\odot}	Measured far-IR luminosity / L_{\odot}
3C293	$(0.67 - 1.0) \times 10^{10}$	$(4.3 - 8.7) \times 10^9$	1.5×10^{10}
3C305	$(2.4 - 2.6) \times 10^{10}$	$(1.8 - 2.3) \times 10^{10}$	1.3×10^{10}

Table 4. YSP bolometric luminosities calculated over the wavelength range 0 – 30,000 Å. The range corresponds to the range of models that provide an acceptable fit to the spectra. Also shown (third column) are the luminosities absorbed or scattered by dust in the nuclear regions, calculated from the amount of reddening required in the best-fitting models. The final column shows the (60 – 100 μm) far-IR luminosities, calculated from the IRAS results of Golombek et al. (1988).

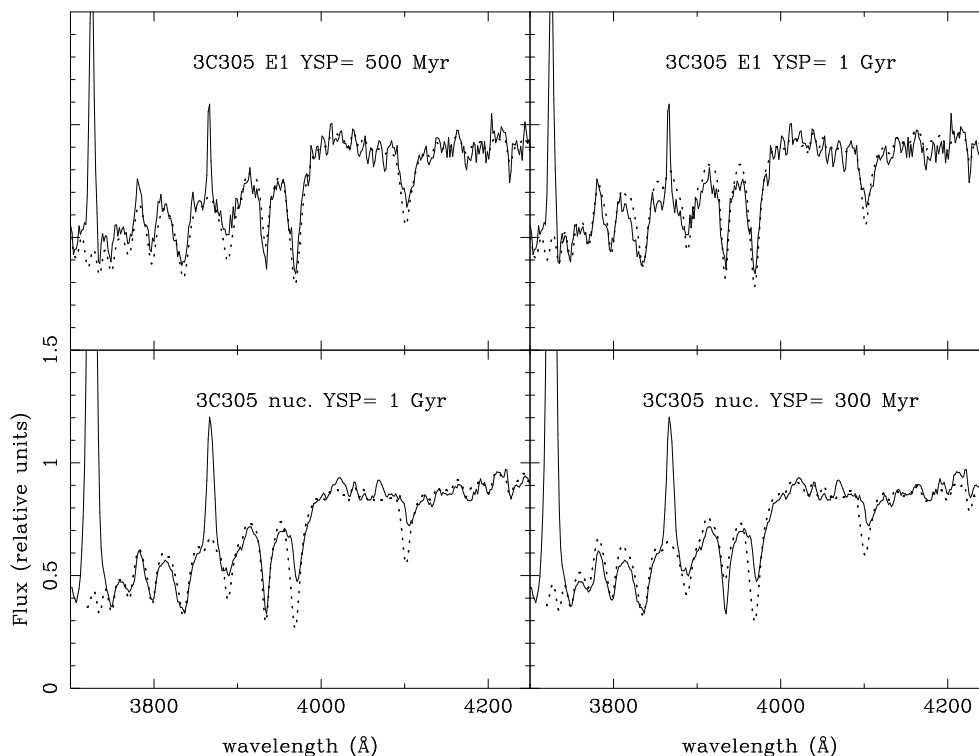


Figure 11. Detailed fits to the nuclear (bottom) and E1 (top) spectra of 3C305 for different YSP contributions and ages. In each case the solid line shows the spectrum of the source, and the dotted line the model fit. The different models are as follows. Lower left: nuclear spectrum with 70% 1 Gyr YSP plus 30% elliptical model. Lower right: nuclear spectrum with 35% 0.3 Gyr YSP plus 65% elliptical model. Upper left: E1 spectrum with 50% 0.5 Gyr YSP plus 50% elliptical model. Upper right: E1 spectrum with 20% 1 Gyr YSP plus 80% elliptical model. The relative proportions of the different components are determined in a normalising bin at 4700Å.

has a relatively large low mass cut-off, would lead us to overestimate the total mass of the starburst component. For example, if the lower mass cut-off of the IMF was at $1.0M_{\odot}$ rather than $0.1M_{\odot}$, or the IMF had a steeper, Scalo power-law index (-3.3), then the assumptions we have used above will lead us to overestimate the total mass in the YSP by a factor $\sim 2 - 3$. The study of the IMF shape for clusters in nearby merger systems is in its infancy. However, despite the controversial result of Smith & Gallagher (2001) for the cluster M82-F, recent results for the Antennae merger system are consistent with either a Salpeter or Scalo IMF with lower mass cut-off at $0.1M_{\odot}$, or a Salpeter IMF with lower mass cut-off at ~ 1.0 (Mengel et al. 2002). Therefore, the results in Table 3 are unlikely to be uncertain by more than a factor of $\sim 2 - 3$.

Overall, despite uncertainties related to the assumptions of spectral synthesis modelling procedure, we believe that the general results listed in section 4.4 are likely to hold.

5 DISCUSSION

5.1 The nature of the young stellar populations

In the following we will assume that the YSP represent post-starburst stellar populations, and that the starbursts have been triggered by galaxy mergers or interactions. However, alternative possibilities include the capturing of the YSP associated with the disks of one or more of the merging

galaxies, and/or the jet-induced star formation associated with the activity.

In the case of captured stellar population, the ages of the YSP reflect the star formation histories of the disks prior to the mergers, and cannot be used to estimate the time scales and order-of-events in the mergers that trigger the activity. Although we cannot entirely discount this possibility, it seems unlikely given that: (a) the masses of the YSP are large; (b) much of the star formation is concentrated within a few kpc of the nuclei of the host galaxies; and (c) the ages of the YSP in the extended regions are similar to those in the nuclear regions. If all the YSP were captured in these objects, then it is unlikely that they would be so strongly concentrated in the nuclear regions. On the other hand, circum-nuclear starbursts are predicted by models for gas-rich mergers, since tidal torques associated with the mergers concentrate gas in the near-nuclear regions. Indeed, CO observations provide direct evidence for large gas concentrations in the nuclear regions of 3C293 and PKS1345+12 (Evans et al. 1999a,b).

In the case of jet-induced star formation, there are three aspects that make this scenario unlikely. First, the ages of the YSP are significantly larger than the expected ages of the high surface brightness radio sources (see section 5.4 below). Second, the published optical, UV and radio images show no clear morphological association or alignment between radio and optical/UV continuum features. Finally, the YSP extend well beyond the maximum extent of the high surface brightness radio structures for the slit PAs used for the ob-

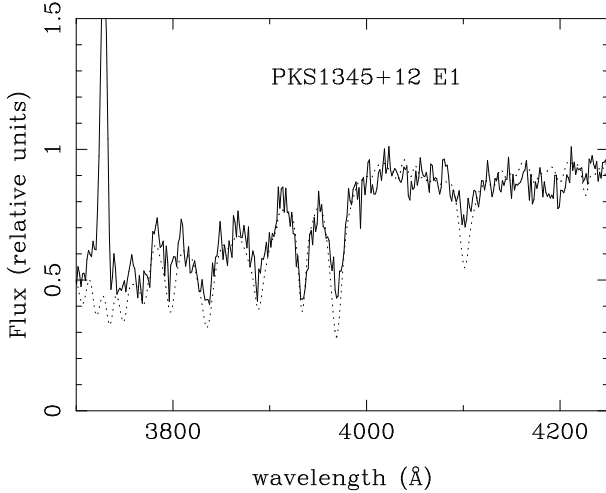


Figure 12. Detailed fit to the e1 spectrum of PKS1345+12 for a 60% 0.7 Gyr YSP plus elliptical model. The relative proportions of the different components are determined in a normalising bin at 4700Å.

servations of all three objects. The only possibility that we cannot entirely exclude is that the YSP are associated with past cycles of radio activity. However, given the general lack of evidence for jet-induced star formation in the population of radio galaxies, we regard this possibility as unlikely.

We conclude that the YSP in the nuclear regions of 3C293 and 3C305 represent post-starburst stellar populations, and that the YSP in the extended regions of these two galaxies are also likely to represent post-starburst populations since their ages are similar to those in the nuclear regions. PKS1345+12 is a less certain case because we have not yet been able to compare the age of its circum-nuclear starburst with that of the extended YSP detected in our observations. However, even if the YSP in the extended region of PKS1345+12 are captured, this is still consistent with the idea that we are witnessing a major merger in which one of the galaxies has a substantial disk component.

5.2 Evolutionary status

The large proportional contribution of the YSP to the total stellar masses of the host galaxies implies that we are witnessing the aftermath of major mergers between massive galaxies, at least one of which must have been gas-rich. It is likely that these major mergers have triggered both the starbursts and the AGN activity, although not necessarily at the same time (see section 5.4 below).

It is interesting to consider these results in the context of the evolution of the population of early-type galaxies. Hierarchical galaxy evolution models suggest that a subset of the elliptical galaxy population was formed and/or has undergone substantial evolution via major mergers at relatively recent epochs (e.g. Kauffmann, Haehnelt & White 1996). Observationally, the recent evolution of the elliptical galaxy population is supported by measurement of line-strength indices in some early-type galaxies that imply the presence of significant YSP (see Kuntschner 2000 and references therein). In addition, infrared studies of ULIGs demonstrate that at least some remnants of major merg-

ers have kinematic properties similar to those of early-type galaxies (Genzel et al. 2001). On the other hand, the interpretation of the redshift evolution of the number density of early-type galaxies is more controversial (e.g. Zepf 1997, Cimatti et al. 2002, Rodighiero et al. 2002), and it is unlikely that *all* early-type galaxies have undergone major evolution in recent past. Indeed, the evidence suggests that both the formation epoch and speed of the evolution of early-type galaxies depend on environment (e.g. Menanteau, Abraham & Ellis 2002). Whereas much of the observational evidence for the recent evolution of the early-type galaxy population is confined to the field, or relatively low luminosity E/SO galaxies on the periphery of clusters (Kuntschner 2000), giant elliptical galaxies in rich clusters show little evidence for recent evolution.

Therefore it is plausible that the three radio galaxies discussed in this paper are associated with the subset of the early-type galaxy population in relatively low density environments that is undergoing the most rapid evolution via mergers in the local universe. The fact that none of the three galaxies is in a rich cluster environment is consistent with this hypothesis.

5.3 A link between ULIGs and radio galaxies?

The status of the radio galaxies in our sample as merging systems raises the issue of whether all merging systems that end up as early-type galaxies go through a radio galaxy phase as part of their evolution. Therefore it is interesting to investigate the links between the radio galaxies, luminous infrared galaxies (LIGs: $L_{\text{IR}} > 10^{11} L_{\odot}$) and ultraluminous infrared galaxies (ULIGs: $L_{\text{IR}} > 10^{12} L_{\odot}$) – some of the most extreme merging systems in the local universe (see Sanders & Mirabel 1996 for a review). The evidence for such links includes the following.

- **Optical morphologies.** In terms of their optical morphologies there are clear similarities between radio galaxies and ULIGs. The three galaxies in our sample form part of the subset of $\sim 50\%$ of all nearby powerful radio galaxies that show evidence for morphological features such as tidal tails, arcs, bridges, and double nuclei that are characteristic of mergers (Heckman et al. 1986). These features have a higher surface brightness than the faint shell structures commonly detected in nearby “normal” elliptical galaxies. Therefore, in terms of the degree of morphological disturbance, radio galaxies fall between ULIGs, which show such high surface brightness features in $>95\%$ of cases (Sanders & Mirabel 1996), and normal elliptical galaxies in which such features are much rarer.

- **Far-infrared luminosities.** Only $\sim 30\%$ of powerful radio galaxies at low redshifts $z < 0.3$ were detected at far-IR wavelengths by the IRAS satellite (Golombek et al. 1988, Impey & Gregorini 1993, Heckman et al. 1994); and, apart from a few rare exceptions, the far-IR luminosities of the detected sources are well below those of ULIGs. This implies that, if a substantial proportion of ULIGs go through a radio galaxy phase, the radio galaxy phase cannot be co-eval with the ULIG phase in all objects. It is notable that, in line with previous results which suggest a strong link between optical/UV starburst activity and far-IR luminosity in radio galaxies (Tadhunter et al. 2002, Wills et al. 2002),

all three of the objects in our sample were detected by IRAS, albeit covering a wide range in far-IR luminosity. Whereas PKS1345+12 is one of the few radio galaxies in the local universe classified as a ULIG based on its far-IR luminosity, the other two sources – 3C293 and 3C305 – have far-IR luminosities that are orders of magnitude lower. However, we showed in section 4.4 that, assuming instantaneous starbursts and complete reprocessing of the optical/UV light by dust, both of these objects would have appeared as LIGs or ULIGs in the past. Even allowing for the fact that the starbursts may not be instantaneous, these results provide clear evidence for a link between radio galaxies and luminous- or ultraluminous infrared galaxies, in the sense that some LIGs or ULIGs may evolve into radio galaxies. This direction of evolution is supported by the fact that the ages of the post-starburst populations in the three objects in our sample are older than those of all the ULIG quasar host galaxies investigated using similar techniques by Canalizo & Stockton (2001).

- **Space densities.** By integrating the $z = 0$ radio luminosity function of Dunlop & Peacock (1990) we find that the space density of extragalactic radio sources in the local universe with radio powers greater than or equal to that of 3C305 ($P_{2.7\text{GHz}} > 5 \times 10^{25} \text{ W Hz}^{-1}$) — the least luminous radio source in our sample — is $\rho(\text{PRG}) = 8.5 \times 10^{-7} \text{ Mpc}^{-3}$ for our assumed cosmology. For comparison the space densities of LIGs and ULIGs, found by integrating the far-infrared luminosity function of Sanders & Mirabel (1996), are $\rho(\text{LIG}) = 2.7 \times 10^{-5} \text{ Mpc}^{-3}$ and $\rho(\text{ULIG}) = 1.2 \times 10^{-7} \text{ Mpc}^{-3}$ respectively. It is notable that the space density of moderately powerful radio galaxies is $\sim 7\times$ greater than that of the ULIGs, but $\sim 30\times$ less than that of LIGs. We also find that the space density of the far-IR sources becomes equivalent to that of the moderately luminous radio sources for $L_{\text{ir}} > 4 \times 10^{11} L_{\odot}$. Even allowing for the fact that not all radio sources may be triggered by major galaxy mergers (see Tadhunter et al. 1989 and Baum et al. 1990 for a discussion), these results are consistent with the idea that all ULIGs and a significant fraction of the LIGs evolve into moderately powerful radio sources. On the other hand, assuming that the timescale of the ULIG/LIG phase is not substantially less than the timescale of the radio source phase, the fact that the space density of radio sources is much larger than that of ULIGs suggests that not all moderately luminous radio sources were ULIGs in the past, although many of them may have been LIGs.

- **Stellar kinematics.** Based on optical spectroscopic data, Heckman et al. (1986) and Smith, Heckman & Illingworth (1990) showed that nearby powerful radio galaxies with strong emission lines have stellar kinematic properties similar to those of “disky” E-galaxies, with relatively large V_c/σ providing evidence for rotational support. These kinematic properties are identical to those deduced from recent near-IR spectroscopic observations that penetrate the dusty environments of the bulges of ULIG galaxies (Genzel et al. 2002); the mean velocity dispersions measured for the ULIGs studied by Genzel et al. (2001: $\langle \sigma \rangle = 185 \pm 14$) are similar to those measured for the radio galaxies with strong emission lines by Smith et al. (1990: $\langle \sigma \rangle = 209 \pm 13$).

Overall, several lines of evidence are consistent with the idea that ULIGs and LIGs can evolve into radio galaxies.

Further studies of the stellar populations in ULIGs, LIGs and radio galaxies would help to put this putative evolutionary sequence onto a firmer footing.

5.4 Triggering and order-of-events

An intriguing feature of the results obtained above is that the post-starburst stellar populations in all of our sample objects are relatively old ($\sim 0.5 - 2.5$ Gyr) compared with the lifetimes of the radio sources estimated from standard spectral ageing arguments (< 0.1 Gyr). Taken at face value this result implies that the radio sources are triggered relatively late in the merger sequence – much later than the starbursts. This ties in with results based on HI 21cm and CO imaging observations, which also suggest a substantial delay between the start of the merger and the triggering of the jets (Evans et al. 1999a,b, Morganti et al. 2003).

What causes the apparent time lag between the starburst and jet triggering events? One possibility is that the lag represents a settling timescale: the time taken for the gas to establish a steady accretion flow into the nuclear regions after it has been stirred up in a major circum-nuclear starburst. Alternatively, the lag may represent the time required to form the type of AGN that is capable of powering powerful relativistic jets. For example, it has been suggested that powerful radio jets are associated with rapidly spinning black holes formed by the coalescence of the black holes in the nuclei of two galaxies undergoing a major merger (Wilson & Colbert 1995). In this case, the starburst/radio source time lag may be related to the coalescence timescale for the binary black hole.

Before leaving this topic it is important to add a caveat about the radio source ages. Recently, the standard spectral ageing estimates of radio source lifetimes have been challenged by Blundell & Rawlings (2001) who argue that radio lobes may be continually replenished by energetic electrons, so that the high frequency breaks/curvature in the radio spectrum may not reflect the ages of the radio sources. In this case, the most extended double radio sources may be much older (0.1 – 1 Gyr) than predicted by traditional spectral ageing arguments. However, two of the sources in our sample are compact radio sources and, for such sources, spectral ageing arguments are thought to provide accurate radio source lifetimes because they agree with dynamical age estimates. Therefore, at least for the two compact objects in our sample, it is difficult to escape the conclusion that there is a substantial time lag between the starburst that produced the YSP we now observe at optical wavelengths, and the triggering of the currently observed radio jets.

Another possibility is that the radio sources have undergone multiple epochs of activity, with one epoch coincident with the original starburst. Indeed, the multiple epochs idea is supported by the detection of low surface brightness extended radio emission surrounding the much higher surface brightness compact radio sources in some objects, including PKS1345+12 (Stanghellini et al. 2001). Moreover, the “double-double” radio structure of 3C293, may also suggest multiple epochs of activity. However, if radio jets are always triggered at the same time as the original merger-induced starbursts, observations of larger samples of radio galaxies should reveal the presence of YSP with relatively young ages (< 0.1 Gyr) in at least some sources.

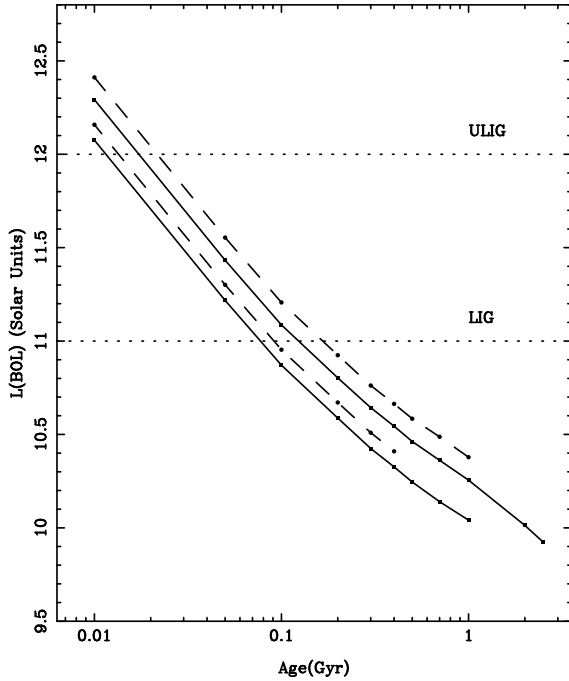


Figure 13. The evolution of the bolometric luminosities of the YSP components with age for the nuclear region of 3C305 (dashed lines), and the nuclear region plus region E2 of 3C293 (solid lines), as predicted by the BC96 instantaneous burst models. For each object two lines are shown, corresponding to the maximum and minimum age YSP that give acceptable fits to both the SEDs and the CaII K absorption line. For reference, the limiting luminosities for LIGs and ULIGs are also shown (see Sanders & Mirabel 1996).

6 CONCLUSIONS AND FURTHER WORK

The results presented in this paper demonstrate the potential of studies of the young stellar populations for investigating the nature of the events that trigger the activity in radio galaxies, the order of events, the timescales, and the relationship between radio galaxies and other types of active objects such as ULIGs. The main results can be summarised as follows.

- **Nature of the YSP and the mergers.** The YSP are identified with post-starburst populations that are relatively old and massive, and represent a large fraction of the total stellar mass in the regions sampled by our spectra. These results imply that we are observing the aftermath of *major mergers* between massive galaxies, at least one of which must have been a gas-rich disk galaxy.

- **Spatial distribution.** Although the YSP are concentrated close to the nuclei of the host galaxies in at least two of our sample objects, in all cases the YSP are spatially extended on a scale of 1 – 20 kpc.

- **Triggering and timescales.** The fact that the post-starburst populations detected in our sources are relatively old compared with the typical ages of extragalactic radio sources, suggests that the activity associated with the observed high surface brightness radio sources was triggered late in the merger sequence — up to 0.5 – 2 Gyr after the starburst responsible for the YSP.

- **Luminous and ultraluminous infrared galaxies.** Our results point to a strong link between the radio galaxies

and at least a subset of the LIG and ULIG populations; they provide evidence that some LIGs and ULIGs may *evolve into* radio galaxies.

It is now important to extend such studies to larger samples of radio galaxies, in order to put these results on a firmer footing, and investigate whether they hold for the general population of radio galaxies with detected YSP.

Acknowledgments

TR and KW acknowledge support from PPARC. RGD and KW acknowledges support from the Royal Society and by the Spanish Ministry of Science and Technology (MCyT) through grant AYA-2001-3939-C03-01. We acknowledge useful comments from the anonymous referee.

REFERENCES

- Allen, M.G., Sparks, W.B., Koekemoer, A., Martel, A.R., O’Dea, C.P., Baum, S.A., Chiaberge, M., Macchetto, F.D., Miley, G.K., 2002, *ApJS*, 139, 411
- Allington-Smith, J.A., Ellis, R.S., Zirbel, E.L., Oemler, A., 1993, *ApJ*, 404, 521
- Arexaga, I., Terlevich, E., Terlevich, R.J., Cotter, G., Diaz, A.I., 2001, *MNRAS*, 325, 636
- Axon, D.J., Capetti, A., Fanti, R., Morganti, R., Robinson, A., Spencer, R., 2000, *AJ*, 120, 2284
- Baan, W.A., Haschik, A.D., 1981, *ApJL*, 243, L143
- Blundell, K.M., Rawlings, S., 2000, *AJ*, 119, 1111
- Bruzual, A.G., 1983, *ApJ*, 273, 105
- Bruzual, A.G., Charlot, S., 1993, *ApJ*, 405, 538
- Canalizo, G., Stockton, A., 2001, *ApJ*, 555, 719
- Charlot, S., Worthey, G., Bressan, A., 1996, *ApJ*, 457, 625
- Chiaberge, M., Capetti, A., Celotti, A., 1999, *A&A*, 349, 77
- Cimatti, A., di Serego Alighieri, S., Fosbury, R.A.E., Salvati, M., Taylor, D., 1993, *MNRAS*, 264, 421
- Cimatti, A., et al., 2002, *A&A*, 391, L1
- Cohen, M.H., Ogle, P.M., Tran, H.D., Goodrich, R.W., Miller, J.S., 1999, *AJ*, 118, 1963
- Dickson, R., Tadhunter, C., Shaw, M., Clark, N. & Morganti, R., 1995, *MNRAS*, 273, L29
- Draper, P.W., Scarrott, S.M., Tadhunter, C.N., 1993, *MNRAS*, 262, 1029
- Dunlop, J.S., Peacock, J.A., 1990, *MNRAS*, 247, 19
- Evans, A.S., Sanders, D.B., Surace, J.A., Mazzarella, J.M., 1999a, *ApJ*, 511, 730
- Evans, A.S., Kim, D.C., Mazzarella, J.M., Scoville, N.Z., Sanders, A.B., 1999b, *ApJ*, 521, L107
- Genzel, R., Tacconi, J.J., Rigopoulou, D., Lutz, D., Tecza, M., 2001, *ApJ*, 563, 527
- Golombek, D., Miley, G., Neugebauer, G., 1988, *AJ*, 95, 26
- González Delgado, R.M., Leitherer, K., Heckman, T.M., 1999, *ApJS*, 125
- González Delgado, R.M., Leitherer, K., Heckman, T.M., 2001, *ApJ*, 546, 845
- Heckman, T.M., Miley, G.K., Balick, B., van Breugel, W.J.M., Butcher, H.R., 1982, *ApJ*, 262, 529
- Heckman T.M., Smith E.P., Baum S.A., van Breugel W.J.M., Miley G.K., Illingworth, G.D., Bothun, G.D., Balick, G.D., 1986, 311, 526
- Heckman, T.M., O’Dea, C.P., Baum, S.A., Laurikainen, E., 1994, *ApJ*, 428, 65
- Holt, J., Tadhunter, C.N., Morganti, R., 2003, *MNRAS*, 342, 995
- Impey, C., Gregorini, L., 1993, *AJ*, 105, 835

- Jackson, N., Beswick, R., Pedlar, A., Cole, G.H., Sparks, W.B., Leahy, J.P., Axon, D.J., Holloway, A.J., 2003, *MNRAS*, 338, 643
- Kauffmann, G., Charlot, S., White, S.D.M., 1996, *MNRAS*, 283, L117
- Kauffmann, G., Haehnelt, M., 2000, *MNRAS*, 311, 576
- Kuntschner, H., Davies, R.L., 1998, *MNRAS*, 295, L29
- Kuntschner, H., 2000, *MNRAS*, 315, 184
- Lilly, S.J., Longair, M.S., 1984, *MNRAS*, 211, 833
- Madau, P., Ferguson, H.C., Dickinson, M.E., Giavalisco, M., Steidel, C.C., Fruchter, A., 1996, *MNRAS*, 283, 1388
- Melnick, J., Gopal-Krishna, Terlevich, R., 1997, *A&A*, 318, 337
- Mirabel, I.F., 1989, *ApJ*, 340, L13
- Mirabel, I.F., Sanders, D.B., Kazès, I., 1989, *ApJ*, 340, L9
- Mengel, S., Lehnert, M.D., Thatte, N., Genzel, R., 2002, *A&A*, 383, 137
- Menanteau, F., Abraham, R.G., Ellis, R.G., 2001, *MNRAS*, 322
- Morganti, R., Oosterloo, T.A., Emonts, B.H., van der Hulst, J.M., Tadhunter, C.N., 2003, *ApJL*, in press
- Morganti, R., Oosterloo, T.A., Capetti, A., de Ruiter, H.R., Fanti, R., Perma, P., Tadhunter, C.N., Wills, K.A., 2003, *A&A*, 399, 311
- Morganti, R., Oosterloo, T.A., Tadhunter, C.N., Vermeulen, R., Phistrom, Y.M., van Moorsel, G., Wills, K.A., 2004, *A&A*, 424, 119
- Rees, M.J., 1989, *MNRAS*, 239, p1
- Robinson T. G., Tadhunter C. N., Axon D. J., Robinson A., 2000, *MNRAS*, 317, 922
- Rodighiero, G., Franceschini, A., Fasano, G., 2002, *MNRAS*, 324, 491
- Salpeter, E.E., 1955, *ApJ*, 121, 161
- Sanders D. B., Phinney E. S., Neugebauer G., Soifer B.T., Matthews K., 1989, *ApJ*, 347, 29
- Sanders, D.B., Mirabel, I.F., *ARA&A*, 34, 1996
- Schlegel, D.J., Finkbeiner, D.P., Davis, M., 1998, *ApJ*, 500, 525
- Seaton, M.J., 1979, *MNRAS*, 187, 73p
- Shaw M., Tadhunter C., Dickson R., Morganti R., 1995, *MNRAS*, 275, 703
- Smith, E.P., Heckman, T.M., 1989, *ApJ*, 341, 658
- Smith, E.P., Heckman, T.M., 1990, *ApJ*, 348, 38
- Smith, E.P., Heckman, T.M., Illingworth, G.D., 1990, *ApJ*, 356, 399
- Smith, L.J., Gallagher, J.S., 2001, *MNRAS*, 326, 1027
- Stanghellini, C., O'Dea, C.P., Dallacasa, D., Baum, S.A., Fanti, R., Fanti, C., 2001, *A&A*, 377, 377
- Surace, J.A., Sanders, D.B., Vacca, W.D., Veilleux, S., Mazzearella, J.M., 1998, *ApJ*, 492, 111
- Tadhunter, C.N., Fosbury, R.A.E., Quinn, P.J., 1989, *MNRAS*, 240, 225
- Tadhunter, C., Scarrott S., Draper P., Rolph C., 1992, *MNRAS*, 256, 53p
- Tadhunter, C.N., Dickson, R.C., Shaw, M.A., 1996, *MNRAS*, 281, 591
- Tadhunter, C., Dickson, R., Morganti, R., Robinson, T.G., Wills, K., Villar-Martin, M., Hughes, M., 2002, *MNRAS*, 300, 977
- van Breugel, W., Heckman, T., Butcher, H., Miley, G., 1984, *ApJ*, 277, 82
- van Breugel, W., Filippenko, A.V., Heckman, T., Miley, G., 1985, *ApJ*, 293, 83
- Wills, K.A., Tadhunter, C.N., Robinson, T.G., Morganti, R., 2002, *MNRAS*, 333, 211
- Wills, K.A., Morganti, R., Tadhunter, C.N., Robinson, T.G., Villar-Martin, M., 2004, *MNRAS*, in press
- Wilson, A.S., Colbert, E.J.M., 1995, *ApJ*, 438, 62
- Zepf, S.E., 1997, *Nat*, 390, 377
- Zirbel, E.L., 1997, *ApJ*, 476, 489